Internal chaotic sea structure and chaos-chaos intermittency in Hamiltonian systems

D. M. Naplekov [1,*] and V. V. Yanovsky[1,2]

[1]*Institute for Single Crystals, NAS Ukraine, 60 Nauky Avenue, Kharkov, 61001, Ukraine*
[2]*V. N. Karazin Kharkiv National University, 4 Svobody Square, Kharkiv, 61022, Ukraine*

In this paper, we study the inhomogeneity of chaotic sea properties far from islands in billiardlike systems and its influence on distributions of particle's return times. A visibly homogeneous chaotic sea at certain parameters has a nontrivial internal structure, in particular, being divided into two chaotic phases with different properties. These phases are not separated by any obstacles, neither in phase nor in configuration spaces, and are partially overlaying. The emergence of a chaotic sea structure may be explained by the existence of remnants of integrable behavior, like sites of regular trajectories of broken islands of stability built into the chaotic sea. In the case of such chaotic seas, we find distributions of return times with two main sites of exponential decay.

I. INTRODUCTION

Billiard-type systems, owing to the combination of their simple form with complicated, chaotic dynamics, became standard model Hamiltonian systems in chaos theory. To such systems belong both usual billiards [1,2] (where a particle moves inside a closed boundary straightly and reflects following the mirror law) and their connections [3]; open billiards with a hole in the border ([4,5]), billiards with obstacles inside ([6–9]), including a disjoined border, billiards with a "breathing" nonstationary border ([10–12]), placed in a gravitational field [13], etc. As an example of such model systems, it is convenient to study different aspects of chaotic behavior, which are inherent also in systems with a more complex arrangement.

One of the main concepts of the theory of Hamiltonian chaos is the existence of a chaotic sea which is filled with chaotic trajectories evenly and everywhere dense. The idea of ergodicity is connected to this uniformity [14,15], and the chaotic sea is also called an ergodic component of the phase space. There may also be islands of stability, which are regions filled with regular trajectories. This is the case of a mixed phase space. Near the boundary of regular regions, a chaotic trajectory can spend an abnormally long time, so-called "stickiness" of trajectories [16,17]. It does not break ergodicity, which assumes uniform filling at infinite times. Islands of stability are usually separated from the chaotic sea but may be broken and connected with it [18]. There may be several ergodic components in the phase space. They appear as a result of the connection of several billiards [19] or exist as chaotic layers inside islands of stability. If a trajectory visits several phase space regions with different properties, it leads to its intermittency: aperiodic switching of a trajectory behavior.

In the paper, we consider a billiard with an obstacle inside, whose chaotic sea has unusual properties, while also considering a usual billiard with similar dynamics. For some of their parameters, the chaotic sea appears to be divided into two chaotic phases with different properties. A similar division of the ergodic component exists for connected chaotic billiards where chaotic phases are divided geometrically, and each requires only part of the system border. Also, similar behavior is found in Hamiltonian systems with two degrees of freedom (2 df), where trajectory motion is hindered by the partial barriers in the phase space [20,21]. Unlike these cases, in our system these phases coexist in a single indivisible system and are not divided by anything either in configuration or in phase spaces. The most unusual is that in the phase space, they are partially superimposed on one another, and there is a region of intersection of nonzero measure with its own properties. If we make a hole in the border and the system becomes open, a hole will be connected simultaneously with both phases.

One of the often-studied characteristics of open billiard systems is the different kinds of distributions of particle escape (for particles initially inside) or transit (for particles entering through a hole then exiting) times [11,22,23]. In general, such distributions decay exponentially in the case of chaotic behavior and follow sedate decay law in the case of regular behavior [24]. If particles get into the system through a hole, then, as a rule, the precise exponent value is proportional to the hole size and does not depend on its position [25]. Except for the main exponential decay, the same billiard may either possess or not a power-law distribution tail. Its existence depends on the choice of billiard parameters, the choice of the hole position, and the distribution of initial data on billiard particles [26–28]. Distributions of return times may also contain a thin structure [29] which carries a significant amount of information about the system. This thin structure is smoothed on large scales.

The paper is organized as follows. In the first sections, we consider the phase portraits of the system and show that under certain parameters, part of the phase space is occupied by
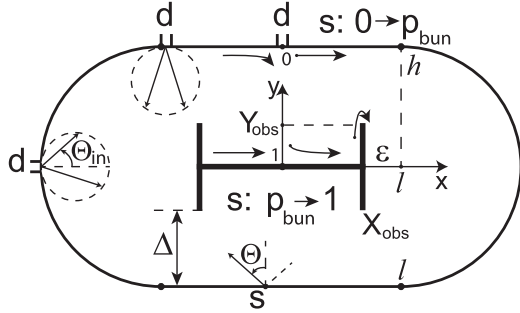
_____
*yanovsky@isc.kharkov.ua

FIG. 1. General view of a stadium billiard with parameters $l = 10$ and $h = 10$ and of an internal obstacle with parameters $X_{\text{obs}} = 6.8$ and $Y_{\text{obs}} = 3.4$. Also shown are border parametrization and three positions of the hole in the border, for which distributions of escape times were considered.

destroyed islands of stability. In the next section, we consider in what order and how evenly over time the points of the trajectory fill the phase portraits and show the existence of subdivision of the chaotic sea into phases. In the last section, we consider the effect of this subdivision on the properties of the system, particularly on the distributions of particle transit times. Understanding the laws of formation of such distributions allows the recovery of the system phase portrait and also the conduction of nondestructive monitoring [30] of systems, inaccessible to direct observations.

II. STADIUM WITH AN OBSTACLE INSIDE

Let us consider a system consisting of the usual billiard with an obstacle inside. Reflections of particles from this obstacle will follow the mirror law in the same way as reflections from the billiard's border. For the billiard, we choose the well-known Bunimovich stadium, whose phase space does not contain islands of stability and is densely filled with chaotic trajectories. An internal obstacle may lead to the emergence of new regular or intermittent trajectories. It also serves as an additional source of chaos, particularly due to the cutting of bunches of trajectories [31]. In the case of an obstacle made from straight-line segments, the bunches of trajectories will be cut by the endpoints of these segments.

The obstacle was chosen in the form of the letter H and located in the center of the billiard. A general view of the considered Bunimovich billiard with an obstacle is shown in Fig. 1. This system is described by four dimensional parameters: l and h for the stadium and X_{obs} and Y_{obs} for the obstacle; up to the scale, it is three dimensionless parameters. It is also convenient to use two additional parameters, namely, $\varepsilon = X_{\text{obs}} - l$ and Δ, which is the value of the gap between the obstacle and the external border (see Fig. 1), equal to $\Delta = h - Y_{\text{obs}}$ for $\varepsilon < 0$ and $\Delta = \sqrt{h^2 - \varepsilon^2} - Y_{\text{obs}}$ for $\varepsilon > 0$. Since the distributions of return times will be further studied, a hole in the border is also considered. This hole is described by two additional parameters: the position of its center on the billiard's border, s_{hole}, and the hole width, d. The distribution of initial data of entering particles is defined by an arbitrary function of the initial particle position and the initial direction of motion. Thus, the distribution of transit times is fully

determined by setting five dimensionless parameters and one two-parameter function.

It is clear that it is almost impossible to conduct a full investigation of such a multiparameter system. Therefore we consider the most natural cases. We fix the parameters of the external billiard at the values $l = 10$ and $h = 10$ andl vary the parameters of the obstacle X_{obs} and Y_{obs}. For the initial distribution of entering particles we choose a uniform particle distribution along the hole and a Lambert distribution of their initial directions of motion $I(s_{\text{in}}, \Theta_{\text{in}}) = I_0 \cos \Theta_{\text{in}}$, where the constant I_0 can be set equal to $I_0 = \frac{1}{2d}$ for normalization and the angle $\Theta_{\text{in}} \in [-\frac{\pi}{2}, \frac{\pi}{2}]$ is counted from the normal to the border. The initial directions of motion, thus, will not depend on the positions of entering particles on the hole. From all possible hole positions, we consider the three most demonstrative cases shown in Fig. 1: a hole in the center of the circular segment of the border, at the edge of the flat border site, and in the center of this site. The hole size d will be the same in all considered cases, respectively, fixed will be the relation of the hole size to the billiard's perimeter for all constructed distributions. This value determines the escape rate in the case of a Bunimovich billiard without an obstacle.

III. PHASE PORTRAITS OF A SYSTEM WITH A DISJOINED BORDER

Let us now consider the phase portraits of the system described above with a closed border. Though the considered system differs from the usual billiard, it is possible to conduct its description in the same way as for billiards. The difference from billiards is that the border is not single-connected. However, the set of all border points is still one-dimensional, therefore, one variable still suffices for the definition of the point's position on the border. We use the border parametrization shown in Fig. 1. Coordinate s is normalized on the total border length $p = 4l + 2\pi h + 4X_{\text{obs}} + 8Y_{\text{obs}}$. We denote $p_{\text{bun}} = (4l + 2\pi h)/p$ and $p_{\text{obs}} = (4X_{\text{obs}} + 8Y_{\text{obs}})/p$ so that $p_{\text{bun}} + p_{\text{obs}} = 1$. The coordinate $s \in [0, 1]$ is counted clockwise along the system border. Tracing of the system border starts from the middle of the upper flat site of the Bunimovich billiard $s = 0$ and proceeds along the border until returning to the initial point $s = p_{\text{bun}}$. Further, similarly, we walk along the perimeter of the obstacle and attribute coordinates $p_{\text{bun}} < s \leqslant 1$ to its points.

Thus, the system border consists of two disjoined components with a common parametrization. The disjoined border leads only to some distinctions in the definition of the distance between two phase space points. These distances are involved, particularly, in the calculation of the Lyapunov exponents. It is necessary to account for the fact that geometrically close trajectory segments may be distant in the phase portrait, and vice versa. However, principal difficulties do not arise.

To build the phase portraits we use Birkhoff coordinates $(s, \sin \Theta)$, defining each trajectory segment by the positions of its beginning s and the sine of the angle of reflection Θ (as shown in Fig. 1), counted from the normal to the border. The determination of the second coordinate $\sin \Theta$ for the obstacle does not differ from that for the usual billiard. Some of the phase portraits in these coordinates are shown in Fig. 2. It
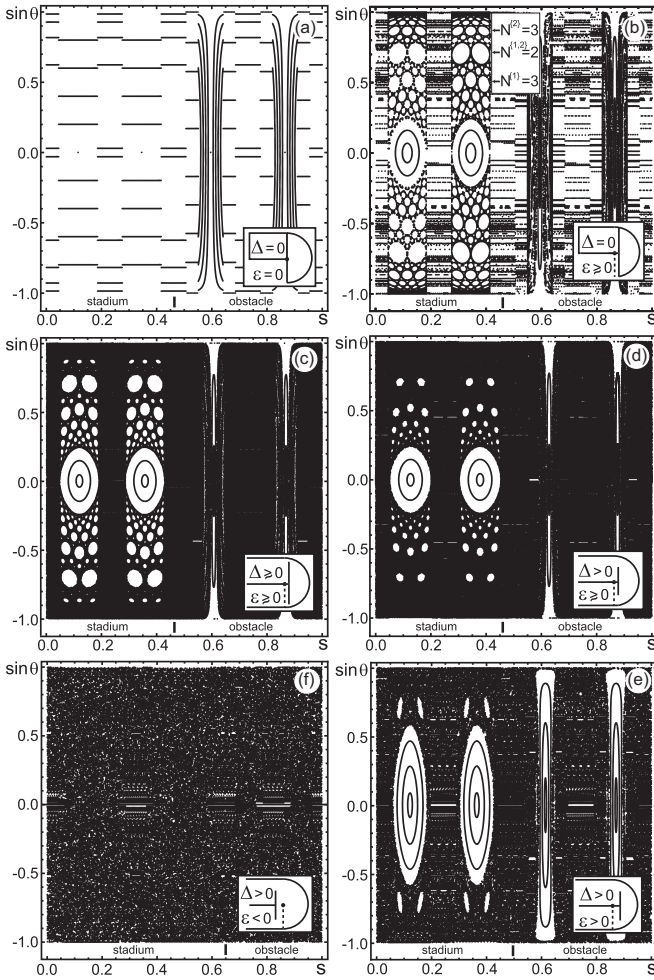
FIG. 2. Phase portraits in Birkhoff coordinates of the system with parameters $l = 10$, $h = 10$. (a) Obstacle parameters $X_{\rm obs} = l$ and $Y_{\rm obs} = h$. The system is equivalent to two separated integrable billiards. (b) Obstacle parameters $X_{\rm obs} = l + \varepsilon$ and $Y_{\rm obs} = h$, with $\varepsilon = 0.3$. Due to the loss of integrability of the circular billiards, a system of islands is formed. (c) Obstacle parameters $X_{\rm obs} = l + \varepsilon$ and $Y_{\rm obs} = h - \Delta$, where $\varepsilon = 0.3$ and $\Delta = 1.0$. The billiards are no longer separated, and the system of islands become partly destroyed. (d) Parameters $X_{\rm obs} = 10.3$ and $Y_{\rm obs} = 7.5$; the gap value Δ increases and the system of islands becomes further destroyed. (e) Parameters $X_{\rm obs} = 12$ and $Y_{\rm obs} = 7.6$; the system of islands is almost destroyed. For $Y_{\rm obs} = 7.2$ there will be only one central island. (f) Typical phase portrait for $\varepsilon < 0$ and $\Delta > 0$; the obstacle parameters are $X_{\rm obs} = 6$ and $Y_{\rm obs} = 4$.

can be seen that the behavior of the system varies from integrable to completely chaotic, depending on the parameters. All trajectories are regular in the case of $\varepsilon = 0$ and $\Delta = 0$ [see Fig. 2(a)], i.e., for the obstacle parameters $X_{\rm obs} = l$ and $Y_{\rm obs} = h$. In this case, the considered system is equivalent to two separated billiards, a rectangle and a half-circle, each of which is integrable. In the case of $\varepsilon > 0$ and $\Delta = 0$, the integrability of these billiards is broken, and for $0 < \varepsilon \ll h$ the destruction of the circular billiard's integrability leads to the emergence of a system of islands of stability. This system is analogous to the KAM theorem system of surviving invariant tori. In this case, the circular billiard's part of the phase portrait consists of a
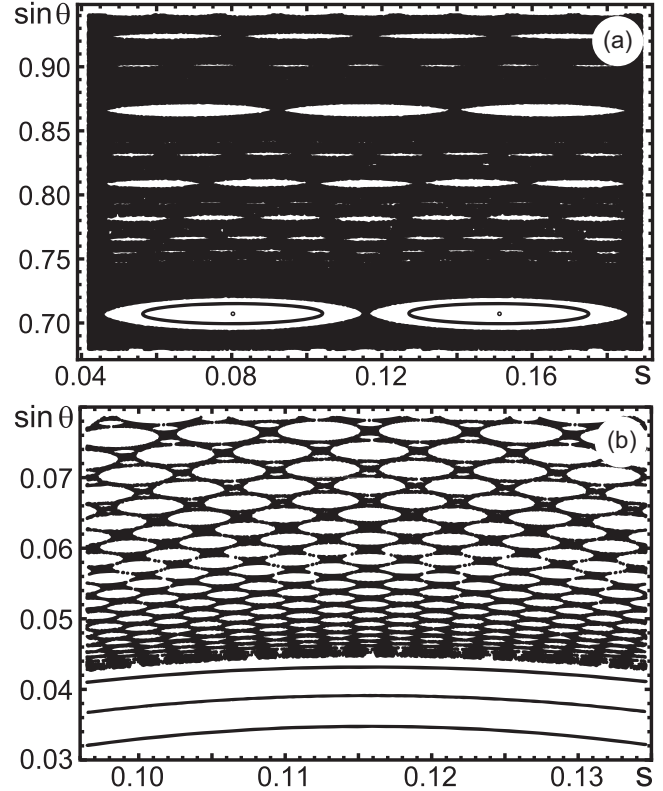

FIG. 3. Some regions of the system of island chains; the parameters of the billiard with an obstacle are $l = 10$, $h = 10$, $\varepsilon = 0.01$, and $\Delta = 0.1$. (a) A system of islands lying above the minimal chain of two islands. (b) A system of islands near the border of the central island.

central island and a set of chains of smaller islands, as shown in Fig. 2(b) and in more detail (for smaller ε and $\Delta \neq 0$) in Fig. 3. A similar system of islands is mentioned in Ref. [32]. The biggest chains by island size lie at

$$\sin \Theta_N^{(1)} = \pm \sin(\pi/2N),$$
$$\sin \Theta_N^{(2)} = \pm \sin(\pi/2 - \pi/2N), \qquad (1)$$

where $N = 2 \ldots N_{\rm max}$ is the number of islands in a chain, and $N_{\rm max}$ depends on the parameters of the obstacle. The chain with the minimal length of two islands is labeled in Fig. 2(b) as $N^{(1,2)} = 2$. Between every two chains of K and $K + 1$ islands lies a chain of $2K + 1$ islands. Between the chains of K and $2K + 1$ islands lies a chain of $3K + 1$ islands. Between the chains of $K + 1$ and $2K + 1$ islands lies a chain of $3K + 2$ islands, etc. In this way, a whole hierarchy of island chains is formed, with each subsequent level consisting of longer chains. There are two such chain systems in the phase portrait. One is above and the other below the chain of two islands. For example, in Fig. 2(b), two chains of three islands, $N^{(1)} = 3$ and $N^{(2)} = 3$, are marked. An example of the chain system for $\varepsilon = 10^{-3}h$ is shown in Fig. 3. The smaller the value of ε, the more elongated the island forms are and the closer the location of their centers to the straight line. With an increase in ε, the central island grows, and the system of chains is deformed and gradually disappears.
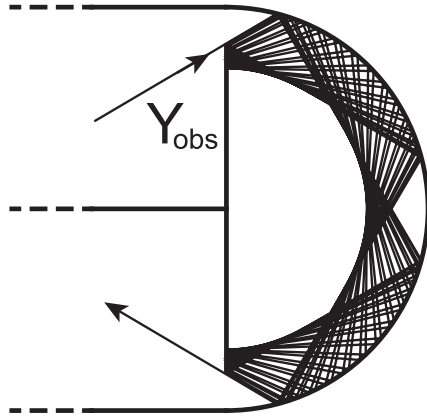
FIG. 4. With a decrease in the parameter Y_{obs}, part of the system's border disappears. Islands of stability are gradually destroyed Their trajectories become connected with the chaotic sea. Shown is an example of a trajectory getting from a chaotic sea to the destroyed part of an island and returning to the sea.

With the appearance of a gap $\Delta > 0$, the integrability of the half-circle and rectangular billiards is violated one more time in a different way, due to the possibility of trajectory transfers from one billiard to another. Even in the case of $\varepsilon = 0$ for $\Delta > 0$, the system will no longer be integrable. At $\varepsilon > 0$, the appearance of a gap $\Delta > 0$ causes the islands to be partially destroyed. This is a consequence of the fact that part of the border disappears, in collisions which were part of some or possibly all of the island's trajectories. The destroyed parts of the islands became connected with the chaotic sea, as shown in Fig. 4. With an increase in the parameter Δ, the islands will consistently diminish in size and disappear from the phase portrait. In Fig. 2(c) for the value $Y_{obs} = 9$, the system of islands is still present below the minimal chain but is almost completely destroyed above it. These chains for $Y_{obs} = 9.9$ are shown in Fig. 3(a). For $Y_{obs} = 7$ the minimal chain is destroyed, and the underlying system of chains is destroyed partially, as shown in Fig. 2(d). With a further increase in ε and Δ, only one central island remains in the phase portrait. A typical phase portrait for this case is shown in Fig. 2(e). The islands around the central one, which are still visible in this phase portrait, will be completely destroyed and disappear with a reduction of Y_{obs} from $Y_{obs} = 7.6$ to $Y_{obs} = 7.2$. In the case of $\varepsilon < 0$, the phase portrait is almost completely occupied by chaotic sea, as shown, for example, in Fig. 2(f). Also visible are areas of unstable periodic trajectories, which arise due to the motion between parallel flat border sites.

The system of islands is more developed for lower values of ε and Δ. This is because the islands are remnants of integrable motion, which takes place at $\varepsilon = 0$ and $\Delta = 0$. The smaller ε is, the more deformed invariant tori survive. It is interesting to note that if one destroys the integrability of a circular billiard in another way, i.e., takes not small positive but small negative ε, which is equivalent to the transfer from a circular billiard to a Bunimovich stadium, then all invariant tori are destroyed immediately. Let us also note that despite analogy with the KAM theorem, this theorem is not applicable in this situation since the system border is not smooth enough. We also note that with the partial destruction of an
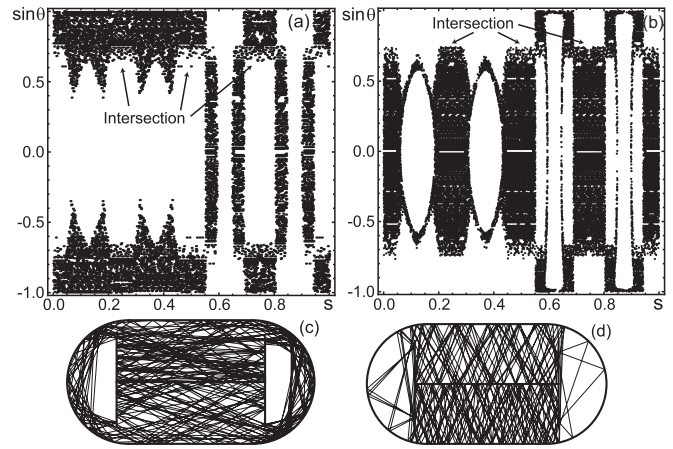

FIG. 5. Phase portraits of two parts of the same chaotic trajectory of length (a) 12 000 and (b) 34 000 iterations. The subdivision of the chaotic sea on two overlaying subareas is visible. Trajectories three hundred iterations long, typical for these subareas (c), (d), are also shown in the configuration space. System parameters are $l = 10$, $h = 10$, $X_{obs} = 12.0$, and $Y_{obs} = 7.2$.

island of stability, the regularity of its trajectories does not disappear completely. Short parts of the former regular trajectories remain and become part of the chaotic sea, as shown in Fig. 4. Therefore, the regularity of motion in the area of the phase space occupied by a destroyed island does not disappear completely, though in the phase portrait, this area looks like the usual ergodic component. Such hidden regularity is the most probable cause of the abnormal chaotic sea properties discussed below.

IV. CHAOTIC SEA SUBAREAS, CHAOS-CHAOS INTERMITTENCY

Usual phase portraits of the system show an entire trajectory simultaneously, but they do not bear information about the order in which the phase portrait was filled with trajectory points. Usually it is considered that a trajectory fills a chaotic sea evenly over time, getting to any area distant from islands with equal probability. However, it turned out that the considered system under certain parameters demonstrates absolutely unusual behavior. The chaotic trajectory stays inside the connected subarea of a chaotic sea for a long time, calculated in tens of thousands of iterations, without visiting the rest of the phase space. An example of such behavior is shown in Fig. 5, where different parts of a single typical chaotic trajectory are shown in both phase and configuration spaces. The full phase portrait of the system with close parameters is shown in Fig. 2(e). As shown in Figs. 5(a) and 5(b), the trajectory fills the chaotic sea unevenly over time, staying for a long time in one or another of its subareas. It can also be seen that these two chaotic sea subareas are superimposed on one another. Thus, there are no obstacles separating them, like chains of islands, for example, that would complicate the transitions from one subarea to another. In configuration space, as shown in Figs. 5(c) and 5(d), the respective trajectory parts are also not divided by any obstacle and are not space separated. Therefore, such division of the chaotic sea differs
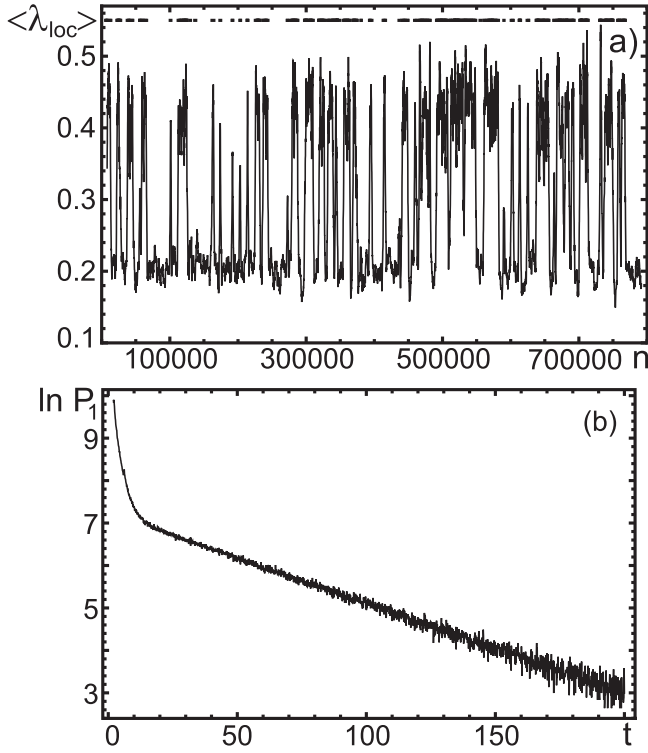
FIG. 6. (a) Dependence of a local Lyapunov exponent value, calculated for different sites of one long chaotic sea trajectory, on the iteration number. The dotted line above shows when the trajectory is in the subarea of the phase space shown in Fig. 5(a). The Lyapunov exponent changes correspond to the transitions of the trajectory between chaotic sea subareas. The system parameters are $l = 10$, $h = 10$, $X_{obs} = 12.0$, and $Y_{obs} = 7.2$. (b) Distribution of the trajectory residence times in the subarea shown in Fig. 5(b).

from one in systems of connected billiards or Hamiltonian systems of 2 df.

The trajectory stays long enough in each of the subareas to make the calculation of characteristics such as the Lyapunov exponent possible. It quantitatively characterizes how chaotic the trajectory is during motion in the given subarea. For this calculation, the usual algorithm was used with the basic trajectory and another one, which were returned to basic after their discrepancy. Each such discrepancy cycle was characterized by the exponent,

$$\lambda_{loc} = \frac{\ln \Delta r_n / \Delta r_0}{\Delta n}, \qquad (2)$$

where r_n is the distance in phase space between the nth trajectory point and the corresponding point of the basic trajectory. The exponential character of the discrepancy of trajectories was also checked. The s axis distance was calculated taking into account the identity of points $s = 0$ with $s = p_{bun}$ for $s < p_{bun}$ and p_{bun} with $s = 1$ for $s > p_{bun}$. The behavior of the mean exponent value of 20 cycles $\langle \lambda_{loc} \rangle$ is shown in Fig. 6(a). There are two characteristic Lyapunov exponent values, which differ more than twice. For the basic trajectory, in which of the two subareas it is located was also traced. The dotted line in Fig. 6(a) shows the cases where it is in the subarea shown

in Fig. 5(a). It is clear that there is an accurate correlation between the value $\langle \lambda_{loc} \rangle$ and the subarea a trajectory is in.

Thus, each of the chaotic sea subareas possesses its own value of the Lyapunov exponent. The subarea shown in Fig. 5(a) is more chaotic; the discrepancy of trajectories there is quicker than in the subarea shown in Fig. 5(b). This is true both in discrete and in continuous time. The distinction of the Lyapunov exponent values is explained by the fact that exponentially rapid discrepancy occurs due to the collisions with the curvilinear parts of the border. Collisions with flat border sites are equivalent to the continuation of rectilinear motion. The share p_{coll} of collisions with curvilinear border sites in the total number of collisions is different for two considered subareas. It depends on the location of the subarea in the phase space. Collisions with curvilinear border sites are the main cause of the discrepancy of trajectories, and the contribution of all other mechanisms can be neglected. Therefore, the difference in p_{coll} in different subareas leads to the corresponding difference in Lyapunov exponents.

A chaotic trajectory consistently passes from one subarea to another, staying in each of them for a possibly long time. The distribution of trajectory residence times for one of the subareas is shown in Fig. 6(b). The duration of residence times from this distribution can be determined only with limited accuracy, particularly because the subareas are overlaying. Since the properties of chaotic sea subareas are significantly different, all chaotic trajectories of the system are intermittent, with chaos-chaos intermittency type. This intermittency differs from one connected with stickiness to the borders of regular motion regions and can coexist with it. Chaos-chaos intermittency was studied earlier for dissipative systems, usually with regard to stochastic or chaotic resonances [33,34], but it was not observed in the billiards (except for stickiness).

The usual billiard in the form of a "mushroom" with two legs was considered to determine whether the emergence of an internal chaotic sea structure is specific to systems with obstacles. Parameters of this billiard correspond to the geometry that is closest to the system considered above with the parameters $l = 10$, $h = 10$, $X_{obs} = 12.0$, and $Y_{obs} = 7.2$. The phase portrait of two parts of the typical chaotic sea trajectory is shown in Fig. 7. In this case, the chaotic sea is also divided into two subareas, with regular transitions of the trajectory from one subarea to another. Thus, chaotic sea subdivision and the emergence of chaos-chaos intermittency are also possible for the usual billiards, without obstacles or connection with other billiards.

To study the chaotic sea properties further, the distributions of Poincaré return times for different areas of the phase space were investigated. The phase space was divided into 200×200 regions of equal volume. A chaotic trajectory repeatedly visits those of these regions that do not lie entirely inside an island. As a result, a sequence of visit times is formed, and, respectively, a distribution of Poincaré return times is formed for each such region. As shown, these distributions for different parts of the ergodic component are significantly different. Three such typical distributions are shown in Fig. 8(d). The main distinctions between these distributions concern short return times, whereas the tails of distributions practically coincide. This results from the fact that for long enough return times the trajectories manage to visit both subareas several
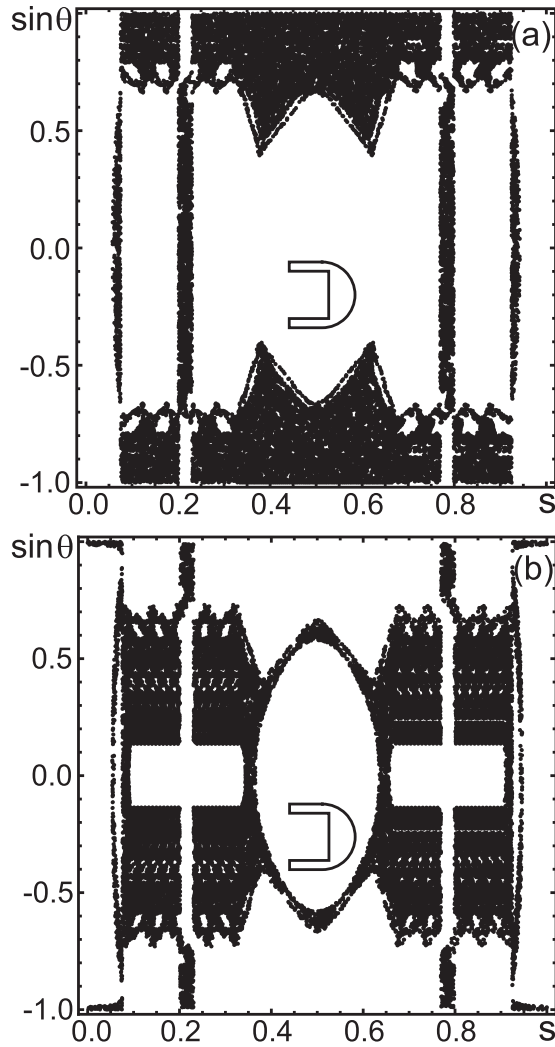
FIG. 7. Phase portraits in Birkhoff coordinates of two different parts of the same chaotic trajectory with lengths of (a) 23 000 and (b) 28 000 iterations for the "mushroom" billiard with two legs. Inset: The form of this billiard. It is visible that the ergodic component of this billiard is also divided into two phases.
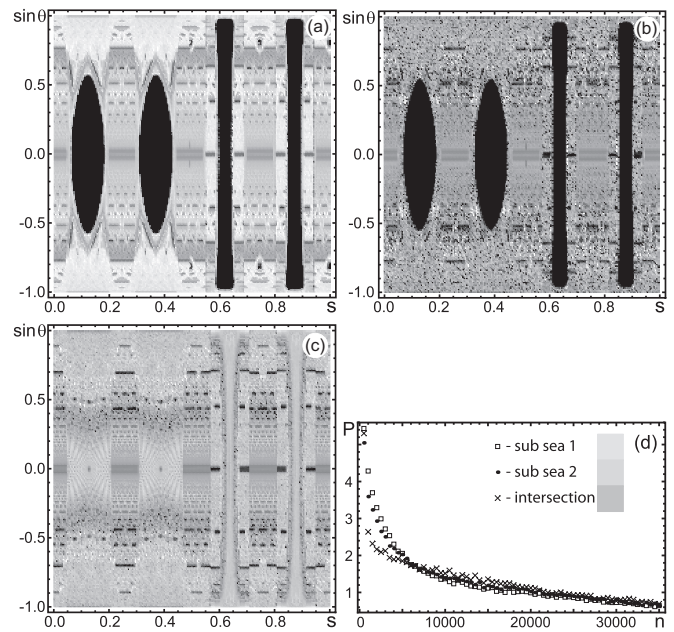

FIG. 8. The map of the special function H characterizes a phase space area based on the analysis of the Poincaré return time distribution for this area. Lighter areas on the map correspond to regions with a higher share of short-time returns. Islands of stability are shown in black. The obstacle parameters are as follows. (a) $X_{\mathrm{obs}} = 12$ and $Y_{\mathrm{obs}} = 7.2$; a large-scale structure of the chaotic sea is visible. (b) $X_{\mathrm{obs}} = 12.0$ and $Y_{\mathrm{obs}} = 6.0$; the chaotic sea is homogeneous. (c) $X_{\mathrm{obs}} = 9.8$ and $Y_{\mathrm{obs}} = 7.0$. The inhomogeneity of the chaotic sea is visible. (d) Typical distributions of Poincaré return times for two subareas and their intersection, with corresponding gray levels.

times, and the distinction of their properties diminishes. On the contrary, for short return times the contribution of trajectories which spend all their time in only one subarea is essential. Such returns reflect properties only of one subarea of the chaotic sea, particularly its phase space volume, not the whole sea.

To construct a map of the phase space on the basis of distributions of Poincaré return times, each of these distributions should be assigned a numerical value which can be reflected by the color of the corresponding phase space area. The standard moments of the distribution, as shown, are not well suited for the visualization of distinctions between considered distributions, which practically match except for their initial part. Moreover, the first moment, i.e., the arithmetic average of return times, is identical all over the chaotic sea and does not show any distinctions between its subareas. For these reasons, we construct a special function $H = \frac{\ln(1+P_2-P_3)}{1+\ln(1+P_1-P_2)}$, where P_1, P_2, and P_3 are the numbers of returns in the intervals $I_1 =$

$[0, 200]$, $I_2 = [1000, 1200]$, and $I_3 = [4000, 4200]$. These intervals are picked up especially for this case, to maximize distinctions between distributions. The sense of the function H is only to visualize the inhomogeneity of the chaotic sea by showing the difference in the distributions of Poincaré return times.

The map of the phase space with values of the function H shown by the gray level is shown in Fig. 8(a). Areas inaccessible to chaotic trajectories are shown in black. Lighter areas on the map correspond to regions of the phase space with a higher share of short-time returns. The lightest regions in Fig. 8(a) match well the subarea of the chaotic sea shown in Fig. 5(a). The region of subareas' intersection, whose distributions differ considerably from the distributions for each subarea, has a darker color on the phase space map and clearly differs. Its location on the map matches the corresponding region in the phase portrait. Thus, the analysis of Poincaré return times also shows the division of the chaotic sea in phases, whose forms match those determined from the phase portraits. The map of Poincaré return times also shows a more complex small-scale internal structure of the chaotic sea.

Figures 8(b) and 8(c) show the phase space maps for other system parameters, constructed absolutely similarly. The parameters $X_{\mathrm{obs}} = 12.0$ and $Y_{\mathrm{obs}} = 6.0$ in Fig. 8(b) correspond to the boundary case where there is practically no division of the chaotic sea yet, but for greater values of Y_{obs}, it already starts to appear. At these system parameters, the chaotic trajectory
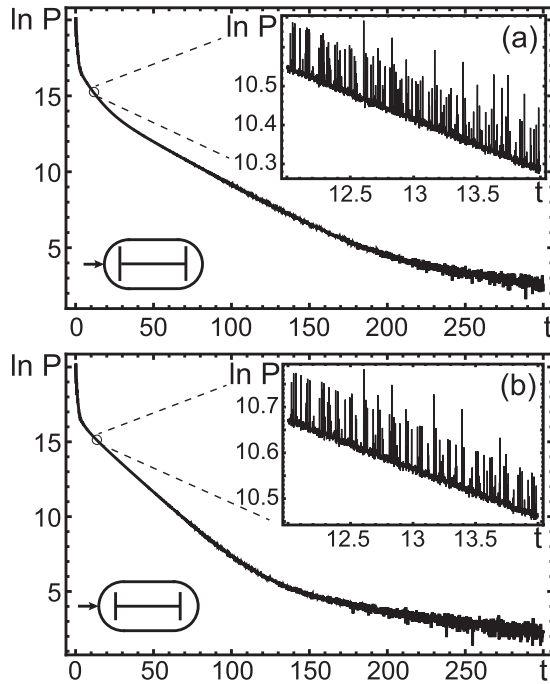
FIG. 9. Distributions of return times for the parameters (a) $Y_{obs} = 7.2$ and (b) $Y_{obs} = 6.0$. The additional site is visible at the beginning of the first distribution. It disappears with the reduction in Y_{obs}. Other system parameters are $l = 10$, $h = 10$, and $X_{obs} = 12$; the hole $d = 0.5$ is at the center of the circular border site, and the number of trajectories $N_{tr} = 4 \times 10^9$. Insets: The small-scale structure of distributions.

almost evenly fills the chaotic sea. It is visible that in this case, on the returns map, there is also no clear subdivision into areas with different properties. Figure 8(c) shows the case of $X_{obs} = 9.8$ where there are no stability islands in the phase space, but the dynamics bear traces of integrable behavior. In this case, as shown, the division of the chaotic sea also takes place, though it is less obviously expressed. The darkest area in Fig. 8(c) corresponds to the region of overlaying of two chaotic sea subareas; these subareas are from different sides of this region. Thus, the existence in the phase space of islands of stability is not a necessary condition for the emergence of chaotic sea subdivision.

V. DISTRIBUTIONS OF ESCAPE TIMES

Let us now consider the system with a hole in the border, through which particles both get into and, after some residence time, leave the system. The arising distribution of transit (return to the hole) times is an often-studied characteristic of open systems. We consider the appearance of these distributions for the case of a chaotic sea with internal structure. In Fig. 9 two distributions are shown, corresponding to the presence and absence of subdivision of phases. The hole is in the center of the circular border site. It is visible that there is a short site of the most rapid descent at the beginning of both distributions, then the main exponential decay and a distribution tail. But the first distribution also has an additional exponential or close site, which is absent in the second

distribution. The first rapid descent site of both distributions is due to the averaged thin structure of these distributions. This structure is mainly concentrated at the beginning of the distributions but also proceeds further. The view of this structure for the next site is shown in the insets in Fig. 9; the thin structure of both distributions is identical. Therefore, the emergence of an additional exponential distribution site is not connected with its reorganization due to the change of system parameters.

For both considered Y_{obs} values, the central island of stability exists in the phase space. It collapses with the hole opening, and the thin structure of considered distributions is mostly connected with the trajectories of this island. To be convinced that the emergence of the additional site is not connected with the central island, distributions of return times only for trajectories with initial data outside of the destroyed central island were developed. Such distributions have no initial site of fast decay but still have an additional exponential site. Distributions of return times for the same system parameters, but two other hole positions, not leading to the destruction of the central island, were also constructed. In both cases, a similar distribution's behavior, though very weakly expressed, took place. This behavior is that the distribution for $Y_{obs} = 7.2$ after the first site decays at first more rapidly, and then more slowly, than the distribution for $Y_{obs} = 6.0$. Thus, the additional site on the distribution in Fig. 9(a) is not connected with the trajectories of the destroyed central island.

The most probable cause of the emergence of an additional site is the internal structure of the chaotic sea, i.e., the existence of two chaotic phases with different properties for the corresponding choice of parameters. For short enough times, a trajectory is unable to visit both subareas several times. At these times, it is possible for a distribution to be defined by the properties of a separate subarea rather than the chaotic sea in general. These times include the typical decay time of considered distributions (for a chosen hole size) as is apparent in Fig. 6(b). The exponent value for an additional site is found to be beyond simple assessment; it depends in a complex, nonlinear way on the hole size. It also depends on the distribution of initial directions of entering particles. Generally, the mechanism of influence of this phase space structure on the distributions of return times, and on other system properties, currently requires additional study.

Further, we consider how the distributions of transit times change with the system parameters. The typical distribution at $X_{obs} < l$ has the main site of exponential decay $P(n) \sim e^{\lambda n}$ and a power-law tail, but with the growth of X_{obs} it may turn into a distribution with two exponential sites and a tail. Two curves describing this transformation with the change in X_{obs} for a fixed value Y_{obs} are shown in Fig. 10(a). The lower curve shows the exponent value of the first distribution site. It was evaluated from the best linear approximation of the distribution on the logarithmic scale in the interval $t \in [t_{min1}, t_{max1}]$. Time intervals for site approximation were within the limits $t_{min1} > 5$ and $t_{max1} < 20$ and did not contain the bend connected with transition to the next site. The upper curve in Fig. 10(a) was constructed similarly, but the intervals for approximation were chosen within $t \in [t_{min2}, t_{max2}]$, $t_{min2} > 75$, and $t_{max2} < 125$. Depending on the value of the parameter X_{obs}, the upper curve is either an exponent of the
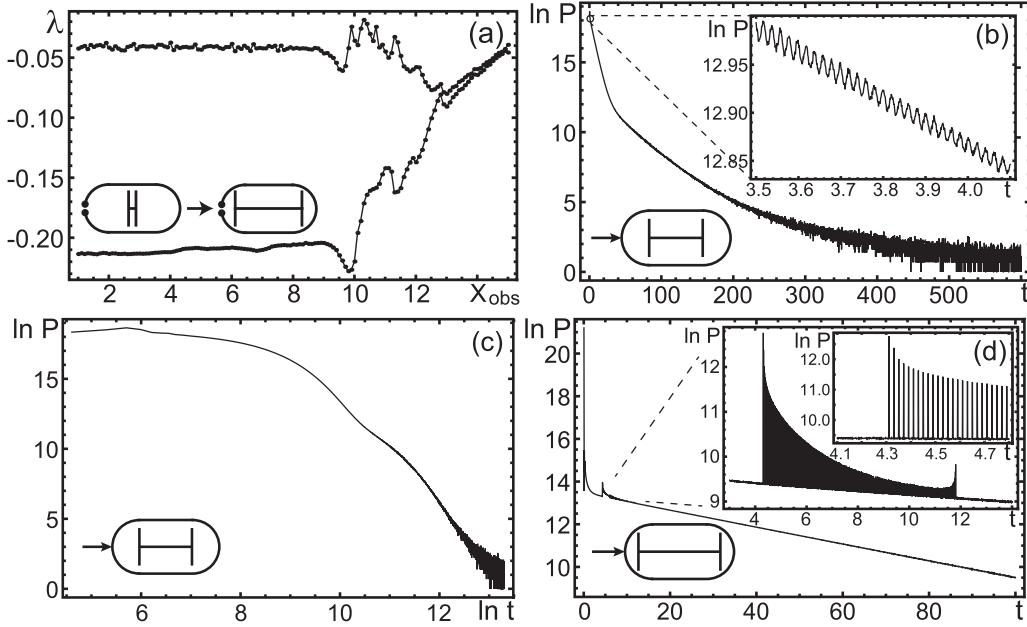
FIG. 10. Transformation of the return time distribution from one site of exponential decay and a tail to two exponential sites and back to one exponential site. (a) Dependence of two distribution angles on the obstacle parameter X_{obs} in the case of the fixed value $Y_{obs} = 7$. The billiard parameters are $l = 10$, $h = 10$, and $d = 0.5$. The hole is in the center of the curvilinear border site. (b), (c) The distribution with two exponential sites for the parameter $X_{obs} = 9.8$ on logarithmic and double-logarithmic scales. Inset: The thin structure of this distribution. The number of trajectories is $N_{tr} = 4 \times 10^9$. (d) The distribution for $X_{obs} = 15$ and $Y_{obs} = 7$ on the logarithmic scale, $N_{tr} = 2 \times 10^9$. In this case, two exponential sites practically merge.

second distribution site or an initial slope angle of the distribution tail. This initial angle is not a main characteristic of the tail, but the definition of its power value requires huge statistics. With smaller statistics, only the initial part of the tail can be confidently determined. Besides, a comparison of exponent and power values is obviously senseless. But it makes some sense to determine the tail's initial slope angle, which at least shows the tail's existence and the presence or absence of its transformations with the change of system parameters.

As follows from Fig. 10(a), the distributions of escape times are almost the same for all X_{obs} less than some value, after which quasiregular behavior and deep reorganization of dynamics begin. At this time, the new distribution site appears. With further growth of X_{obs}, the exponent values of two exponential sites draw together and, starting from some value, practically match. The distribution for the case of the fastest main decay at $X_{obs} = 9.8$ is shown in Fig. 10(b). It is shown that this distribution contains at least three different sites, two of which are close to the exponential law of decay and one of which is the tail. The same distribution on the double-logarithmic scale is shown in Fig. 10(c). Both exponential sites have explicit curvature. The inset in Fig. 10(b) shows the thin structure of this distribution. It essentially differs from the one in Fig. 9. This is natural since, at $X_{obs} = 9.8$, there are no islands in the phase space. The distribution for the greatest admissible value of X_{obs} is shown in Fig. 10(d). More than 80% of all returns in this distribution are concentrated in two peaks lying at the very beginning of the distribution at times $t_{p1} = 2(l + h - X_{obs}) = 0.0204$ (2.5%) and $t_{p2} = 4(l +$

$h - X_{obs}) = 0.0408$ (80.3%). This is explained by the regular character of trajectories of the destroyed central island. It is interesting that the trajectories which lingered on it create the separate distribution site shown in the insets in Fig. 10(d). This site consists of the periodically following distribution peaks and has an explicit beginning and end.

Similarly obtained dependencies for the case of the hole located at the junction of circular and flat border sites are shown in Fig. 11. This case differs from the previous one only in the hole's position. Distributions of return times for this hole position generally consist only of one exponential site and a tail for all values of X_{obs}. A second exponential site with an explicitly different exponent value does not appear. Thus, the division of the chaotic sea into subareas may not lead to the emergence of a new distribution site; it depends also on the position of the hole.

The upper curve in Fig. 11(a) corresponds to the tail of the distribution. It practically does not change with the parameter X_{obs} for the considered hole position. The tail value starts to decrease with an increase in X_{obs} after the reorganization of system dynamics, but not as considerably as in the previous case. The distribution of return times for $X_{obs} = 9.8$ is shown in Fig. 11(b) and on the double-logarithmic scale in Fig. 11(c). It is shown that the distribution tail is sedate; it follows its rectilinear form in Fig. 11(c). The thin structure of this distribution is shown separately in Fig. 11(d).

Some other transformations of transit time distributions with the change in obstacle parameters are shown in Fig. 12. In the case of the hole in the flat border site, the distribution behavior is similar to that considered above. The distribution
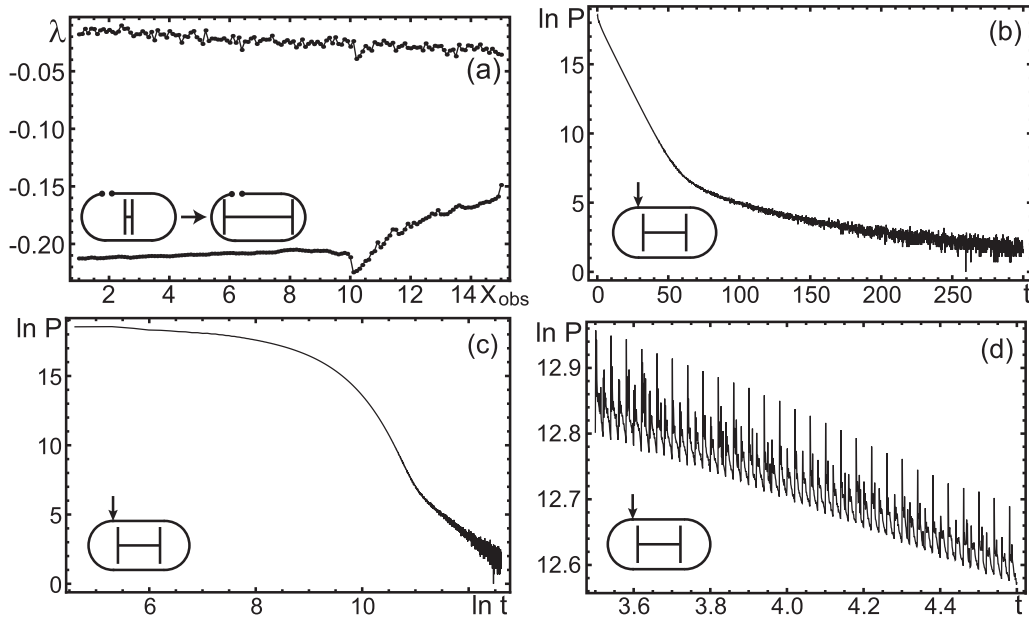
FIG. 11. Transformations of the exponential decay site and a tail of the return time distribution. (a) Dependence of the distribution values on the parameter X_{obs} for the fixed value $Y_{\text{obs}} = 7$. Billiard parameters are $l = 10$, $h = 10$, and $d = 0.5$; the hole is at the junction of the curvilinear and the flat border sites. (b)–(d) Distribution for $X_{\text{obs}} = 9.8$ on logarithmic and double-logarithmic scales and the thin structure of this distribution. The second exponential site does not appear for this position of the hole.

preserves its structure, which is one exponential site and a power-law tail. Their characteristics weakly depend on the obstacle parameters X_{obs} and Y_{obs}. In the case of a hole in the circular border segment, such behavior remains only until values of X_{obs} less than l, or $\varepsilon < 0$. After this, the dynamics of the system changes significantly and one more site of

exponential decay appears at the times where earlier there was a distribution tail. Exponent values at both sites draw together with further growth of X_{obs} until they become almost identical. The obstacle parameters $X_{\text{obs}} = 12.0$ and $Y_{\text{obs}} = 6.0$ correspond to the case of such a merger almost having happened.
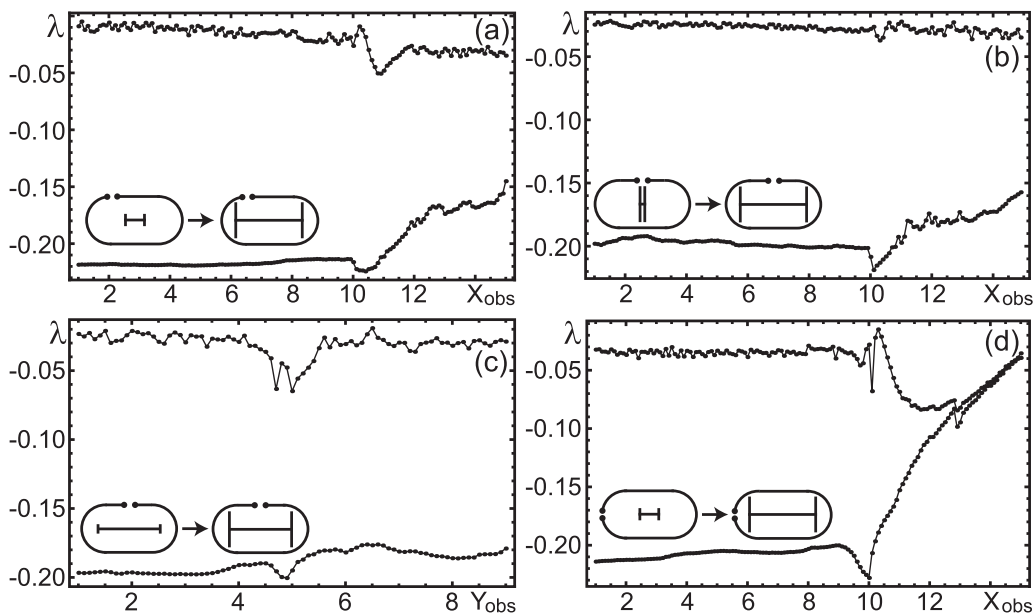

FIG. 12. Dependence of the return time distribution site values (a) on the obstacle parameter X_{obs} for $Y_{\text{obs}} = X_{\text{obs}}/2$, with the hole at the edge of the flat border site; (b) on the parameter X_{obs} at the fixed value $Y_{\text{obs}} = 7$, with the hole in the center of the flat site; (c) on the obstacle parameter Y_{obs} at the fixed value $X_{\text{obs}} = 12$, with the hole in the center of the flat site; and (d) on X_{obs} in the case of $Y_{\text{obs}} = X_{\text{obs}}/2$, with the hole in the center of the circular border site. The billiard parameters are $l = 10$ and $h = 10$; the hole size is $d = 0.5$.

TABLE I. Joint table of transformations of phase portraits, the evenness of their filling, and return time distributions occurring with a change in parameter ε. It is shown that the second exponential decay site and subdivision of the ergodic component in phases appear simultaneously when $\varepsilon \approx 0$ and the system dynamics is close to integrable. This dynamics may not be reflected in the phase portrait. But the existence of remnants of regular motion leads to the emergence of unusual system properties, uneven chaotic sea filling, chaos-chaos intermittency, and additional sites on escape time distributions.

	$\varepsilon < 0$	$\varepsilon \lesssim 0$	$\varepsilon \gtrsim 0$	$\varepsilon > 0$
Phase portrait	No islands	No islands	System of islands	One central island
Filling of chaotic sea	Even	Uneven	Uneven (most explicit)	Even
Escape time distribution	One exponential site	One or two exponential sites	One or two exponential sites	One exponential site

The obtained results are listed in Table I. For values of parameter $\varepsilon \sim 0$, corresponding to the existence of remnants of destroyed regular motion, the system dynamics differs qualitatively from the usual chaotic dynamics. This is manifested both in the uneven filling of phase portraits and in the existence, for certain hole positions, of a second exponential decay site on the distributions of return times. At values of $\varepsilon \lesssim 0$, this change in dynamics is not yet reflected in the phase portrait. However, the unevenness of its filling and an additional distribution site have already appeared. The most explicit division of the chaotic sea into subareas, and, accordingly, the appearance of a chaos-chaos intermittency, was observed in the case of $\varepsilon \gtrsim 0$. Thus, traces or remnants of integrable behavior in the phase space of the Hamiltonian system can lead to the appearance of special chaotic sea properties, intermittency of the chaos-chaos type, and the appearance of additional decay sites on the distributions of return times.

VI. DISCUSSION

Chaos-chaos intermittency is found in many systems, such as one-dimensional cubic mapping and the Chua chain. Usually, this intermittency is associated with the trajectory transitions between the attractors of a dissipative system as a result of external influence. Similar behavior is also found in 2-df Hamiltonian systems, where a chaotic trajectory is confined in a resonance area for a long time and eventually escapes to another resonance area through so-called turnstile structures. However, in billiards, this behavior has not been observed before. This type of intermittency occurs naturally for two connected different chaotic billiards. In this case, the division of the chaotic sea into different phases is trivial and due to purely geometrical reasons.

In our case, this heterogeneity of the chaotic sea is caused by its internal dynamics. In phase portraits, the sea looks homogeneous, not divided into subareas by any obvious phase space structures. The heterogeneity of the properties of the chaotic sea leads to the presence of two exponential decay sites on some distributions of return times. This is also unusual for billiards, including connected ones. In connection with such behavior of the system, many questions currently remain open. In particular, it is unclear what determines the shape of the boundaries of the chaotic sea subareas. These boundaries do not seem to be related to any special trajectories. The exponent values of both exponential decay sites are also beyond simple analytical estimates. Thus, a behavior of Hamiltonian systems (with nonsmooth borders) close to the integrable one is nontrivial and has not been sufficiently studied.

VII. CONCLUSIONS

In this paper, we consider systems that behave unusually when their dynamics is close to an integrable one. Their phase portraits may contain islands of stability, which under certain parameters are arranged in an unusual hierarchy of chains of islands, similar to the surviving KAM tori. This hierarchy of islands either appears or does not, depending on how integrability is broken. In the considered system, these islands are partially destroyed, which leads to the emergence of hidden regularity in the form of sites of the island's regular trajectories built into the chaotic sea.

It turns out that with the system parameters corresponding to the existence of traces of integrable behavior, a chaotic trajectory fills the phase portrait unevenly. The visibly homogeneous chaotic sea appears to consist of two overlaying subseas with different properties. For each subarea, the Lyapunov exponent was calculated; they are considerably different. All chaotic trajectories regularly visit both subareas, passing from one to another after some time of residence. Thus, for certain parameters, all chaotic trajectories of the system are intermittent, with the chaos-chaos intermittency type. Phase space maps were also constructed, characterizing the area based on the analysis of its distribution of Poincaré return times. They also show the inhomogeneity of chaotic sea properties and its division into subareas matching those determined from phase portraits.

Distributions of particle's escape times were considered for several positions of the hole in the border. All the distributions in the case of a homogeneous chaotic sea have one main site of exponential decay and a power-law tail. Distributions for those parameters that correspond to the subdivision of the chaotic sea contain an additional site of exponential decay for one of the considered hole positions. In two other cases, however, this site does not appear. Dependence of the distributions on the system parameters and the thin structure of these distributions were also considered. In some distributions a separate site was found, formed by the system of sharp quasiperiodic distribution peaks.

Thus, in this paper, the possibility of chaotic sea subdivision into phases is shown, as well as the existence, in this case, of return time distributions with two sites of main exponential decay.

[1] Y. G. Sinai, Russ. Math. Surv. **25**, 137 (1970).

[2] L. Bunimovich, Funct. Anal. Appl. **8**, 254 (1974).

[3] G. M. Zaslavsky and M. Edelman, Phys. Rev. E **56**, 5310 (1997).

[4] J. Nagler, M. Krieger, M. Linke, J. Schonke, and J. Wiersig, Phys. Rev. E **75**, 046204 (2007).

[5] E. G. Altmann, J. S. E. Portela, and T. Tel, Rev. Mod. Phys. **85**, 869 (2013).

[6] M. Hentschel and K. Richter, Phys. Rev. E **66**, 056207 (2002).

[7] B. Dietz, A. Heine, A. Richter, O. Bohigas, and P. Leboeuf, Phys. Rev. E **73**, 035201(R) (2006).

[8] T. Shigehara, Phys. Rev. E **50**, 4357 (1994).

[9] S. M. Saberi Fathi, W. Ettoumi, and M. Courbage, Phys. Rev. E **93**, 062216 (2016).

[10] B. Appelbe, Chaos **26**, 113104 (2016).

[11] M. Hansen, R. E. de Carvalho, and E. D. Leonel, Phys. Lett. A **380**, 3634 (2016).

[12] E. D. Leonel and C. P. Dettmann, Phys. Lett. A **376**, 1669 (2016).

[13] M. F. Andersen, A. Kaplan, N. Friedman, and N. Davidson, J. Phys. B: At. Mol. Opt. Phys. **35**, 2183 (2002).

[14] I. G. Sinai, *Topics in Ergodic Theory* (Princeton University Press, Princeton, NJ, 2017).

[15] C. C. Moore, Proc. Natl. Acad. Sci. USA **112**, 1907 (2015).

[16] E. G. Altmann, A. E. Motter, and H. Kantz, Chaos **15**, 033105 (2005).

[17] C. P Dettmann and O. Georgiou, J. Phys. A: Math. Theor. **44**, 195102 (2011).

[18] D. M. Naplekov and V. V. Yanovsky, Phys. Rev. E **94**, 042225 (2016)

[19] L. A. Bunimovich, Chaos **11**, 802 (2001).

[20] J. D. Meiss, Chaos **25**, 097602 (2015).

[21] V. Rom-Kedar and S. Wiggins, Arch. Ration. Mech. Anal. **109**, 239 (1990).

[22] H. Tanaka and A. Shudo, Phys. Rev. E **74**, 036211 (2006).

[23] T. Miyaguchi, Phys. Rev. E **75**, 066215 (2007).

[24] W. Bauer and G. F. Bertsch, Phys. Rev. Lett. **65**, 2213 (1990).

[25] J. D. Meiss, Chaos **7**, 139 (1997).

[26] A. J. Fendrik, A. M. F. Rivas, and M. J. Sanchez, Phys. Rev. E **50**, 1948 (1994).

[27] H. Alt, H. D. Graf, H. L. Harney, R. Hofferbert, H. Rehfeld, A. Richter, and P. Schardt, Phys. Rev. E **53**, 2217 (1996).

[28] C. P. Dettmann and O. Georgiou, Phys. Rev. E **83**, 036212 (2011).

[29] D. M. Naplekov and V. V. Yanovsky, Phys. Rev. E **97**, 012213 (2018).

[30] L. A. Bunimovich and C. P. Dettmann, Europhys. Lett. **80**, 40001 (2007).

[31] S. V. Naidenov, D. M. Naplekov, and V. V. Yanovskii, JETP Lett. **98**, 496 (2013).

[32] J. Chen, L. Mohr, H.-K. Zhang, and P. Zhang, Chaos **23**, 043137 (2013).

[33] S. Sinha and B. K. Chakrabarti, Phys. Rev. E **58**, 8009 (1998).

[34] V. S. Anishchenko, A. B. Neiman, and L. O. Chua, Int. J. Bifurcat. Chaos **4**, 99 (1994).